UDK: 656.7/2:621.43.032:514/539
COSATI: 11-12, 21-11, 01-03

Damage of Turbojet Engine Disks in a Function of Cyclic Material Properties and the Type of Engine Start-Stop Cycle

Strain Posavljak[1)]
Miodrag Janković[2)]
Katarina Maksimović[3)]

The damage of one turbojet engine disk, dominantly exposed to centrifugal forces of blades and its own centrifugal forces, was discussed in this paper. It was assumed that 23H11N2V2MF steel in delivered and heat treatment state would be used for disk manufacturing. One blade and a critical disk area were observed as separated ideal elastic bodies. Their stress response at maximum rotation frequency was determined using the finite element method. Equivalent stress at the critical point of disk was brought in relation to equivalent stress at the corresponding point of disk when observed as a blisk reduced to an axisymmetrical problem. The so-called equivalent stress concentration factor was thus obtained. This factor was used for defining Sonsino-Birger's curve which, in a combination with cyclic stress-strain and Masing's curves, was used for determining spectra of real (elastic-plastic) strain amplitudes at the disk critical point for three different start-stop cycles. These start-stop cycles, defined as blocks of rotation frequency, were decomposed at simple cycles. Spectra of real strain amplitudes, used for that purpose, were brought in relation to Morrow's curves of low cycle fatigue life. Both states of the above mentioned steel of known cyclic properties were taken into account

Key words: **aircraft engine, turbojet engine, disk, material fatigue, cyclic stress-strain, stress concentration, centrifugal force, finite element method.**

Introduction

THE damage of turbojet engine disks presents material degradation during theirs exploitation. The degree and rate of degradation depend on material properties and realized engine start-stop cycles.

Engine start-stop cycles can be described in different ways. For disks, dominantly exposed to centrifugal forces of blades and their own centrifugal forces (fan and compressor disks), engine start-stop cycles are described by blocks of rotation frequency (n) in time (t). These disks work in conditions of low cycle fatigue (LCF) and their cyclic material properties are key properties.

Damage estimation of a particular disk predominantly exposed to centrifugal forces of blades and its own centrifugal forces requires knowing the following: engine start-stop cycles defined by blocks of rotation frequency, cyclic events within these blocks, cyclic properties of material used or nominated for manufacture and stress-strain response at the critical point or the point of expected crack initiation. The disk observed in this paper is the first stage low pressure compressor rotor disk of the R25-300 turbojet engine.

Engine start-stop cycles

Three blocks of rotation frequency (blocks A, B and C) of the first stage low pressure compressor rotor, of the R25-300 turbojet engine, in Fig.1, was taken into account [1]. The block A presents one engine ground control and the blocks B and C present two training flights.

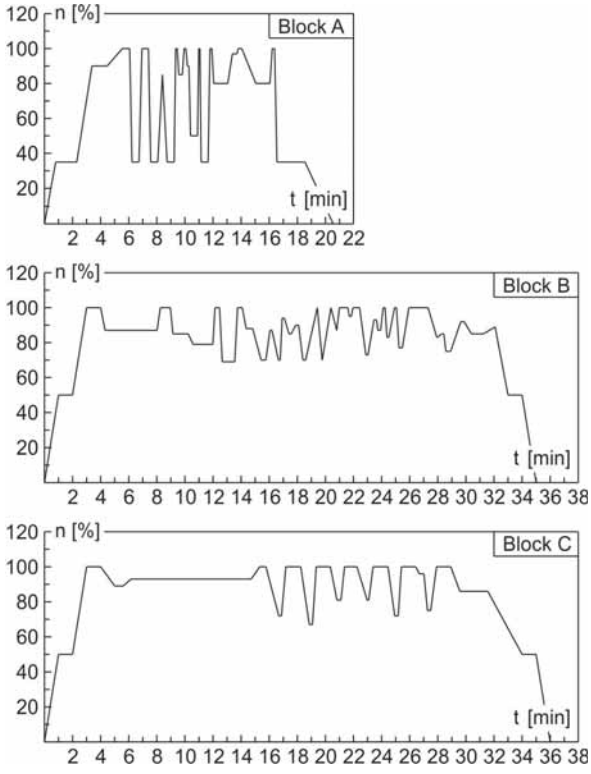

Figure 1. Blocks of rotation frequency of the first stage low pressure compressor rotor, of the R25-300 turbojet engine

[1)] University of Banja Luka, Faculty of Mechanical Engineering, Bul. Vojvode Stepe Stepanovića 75, 78000 Banja Luka, Republic of Srpska, BOSNIA AND HERZEGOVINA
[2)] University of Belgrade, Faculty of Mechanical Engineering, Kraljice Marije 16, 11120 Belgrade, Serbia
[3)] City Administration of City Belgrade, Secretariat for Utilities and Housing Services Water Management, Kraljice Marije 1, Belgrade, SERBIA

Cyclic events

The blocks, shown in Fig.1, were satisfyingly modified and decomposed to cyclic events here presented as X-Y-X cycles of rotation frequency. The decomposition was carried out using the "reservoir" method [1,2] which, applied for the block B, is shown in Fig.2.

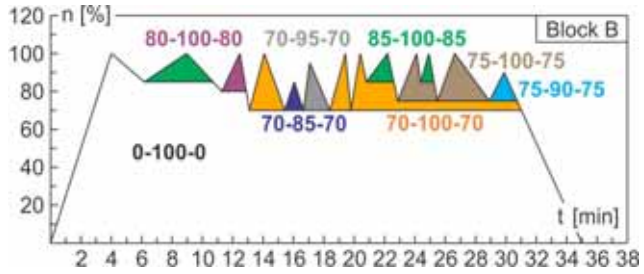

Figure 2. "Reservoir" method applied for the block B

The X-Y-X cycles within the blocks A, B and C, sorted according to the level (i) and the number of appearance (N_i), are included in Table 1.

Table 1. X-Y-X cycles of rotation frequency within the blocks A, B and C

Block A			Block B			Block C		
i	X_i - Y_i - X_i	N_i	i	X_i - Y_i - X_i	N_i	i	X_i - Y_i - X_i	N_i
1	0-100-0	1	1	0-100-0	1	1	0-100-0	1
2	35-100-35	3	2	70-100-70	3	2	70-100-70	3
3	50-100-50	1	3	75-100-75	2	3	75-100-75	1
4	80-100-80	2	4	80-100-80	1	4	80-100-80	2
5	85-100-85	1	5	85-100-85	3	5	90-100-90	1
6	35-85-35	1	6	70-95-70	1			
			7	75-90-75	1			
			8	70-85-70	1			

Cyclic material properties

Material used for manufacturing the first stage low pressure compressor rotor disk of the R25-300 turbojet engine is 13H11N2V2MF steel. The cyclic properties of this steel in delivered and heat treatment state (Heating at 1000°C, Oil quenching, Tempering at 640°C, Air cooling) obtained experimentally [1], are given in Table 2.

Table 2. Cyclic properties of 13H11N2V2MF steel in delivered state (DS) and heat treatment state (HTS)

Property	Value	
	DS	HTS
Modulus of elasticity, E [MPa]	206682.0	229184.6
Cyclic strength coefficient, K' [MPa]	1103.0	1140.0
Cyclic strain hardening coefficient, n'	0.118	0.0579
Fatigue strength coefficient, σ'_f [MPa]	1818.8	1557.3
Fatigue strength exponent, b	-0.144	-0.0851
Fatigue ductility coefficient, ε'_f	0.5351	0.3175
Fatigue ductility exponent, c	-0.6619	-0.7214

Stress-strain response at the critical disk point

For determining the stress-strain response at the critical disk point, it was enough to observe one blade and one critical disk area (at first as ideal elastic bodies). The linear stress response of the blade and the nodal reactions at the blade root contact surfaces, at the maximum rotation frequency n = 100% (186 s^{-1}), were obtained using the finite element method [1, 3] (FEM). Using the FEM and the same rotation frequency, the mentioned reactions in a transformed form were used as nodal forces for obtaining a linear stress response of the critical disk area. The axisymmetrical linear stress response of the disk, when observed as blisk (**bl**aded d**isk**), was also obtained (see Fig.3). The modulus of elasticity E=229184.6 MPa, Poison's coefficient ν=0.29, shear modulus G=88831.24 and mass density ρ=7820 kg/m^3, of 13H11N2V2MF steel in heat treatment state, were assigned to all FEM models.

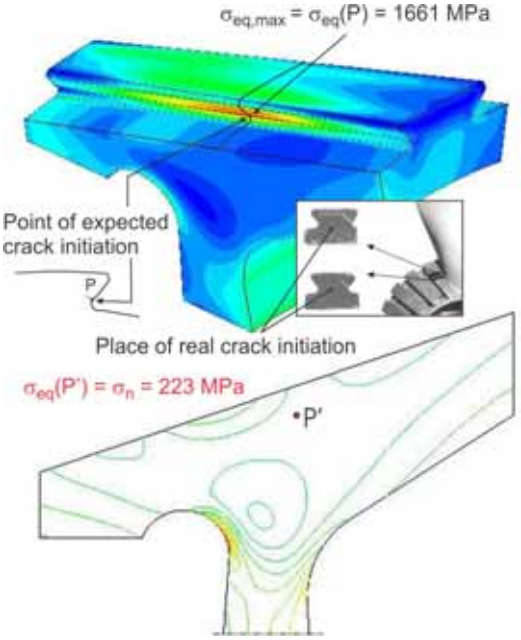

Figure 3. Linear stress response of the critical disk area (above) and the linear axisymmetrical stress response of the same disk when it is observed as a blisk (down)

According to Fig.3, the maximum equivalent stress $\sigma_{eq,\max}$ at the point of expected crack initiation (critical point P) and the corresponding strain are unreal (the mentioned stress is much higher than the tensile strength R_m=1000 MPa of 13H11N2V2MF steel in heat treatment state). It can be seen that the critical point P corresponds to a real crack initiation. The equivalent stress at the point P' of blisk, which corresponds to the critical disk point P, taken as the nominal stress σ_n, was used for the calculation of a so-called equivalent stress concentration factor $K_{eq} = 7.45$. This factor, defined as the ratio of $\sigma_{eq,\max}$ and σ_n served for the transformation of the linear stress-strain response at the critical disk point, into a nonlinear one. Respecting memory of metals, the nonlinear stress-strain response at the critical disk point, using Sonsino-Birger's approach, was here described by stabilized hysteresis loops assigned to all cycles of rotation frequency contained in Table 1. Sonsino-Birger's approach [4, 5, 6] presents one of Neuber's rule modifications. This approach is based on the solution of the following systems of equations.

$$\varepsilon = \frac{1}{2}\frac{K_{eq}\cdot\sigma_{ni}}{E}\left(\frac{K_{eq}\cdot\sigma_{ni}}{\sigma}+1\right)$$
$$\varepsilon = \frac{\sigma}{E}+\left(\frac{\sigma}{K'}\right)^{\frac{1}{n'}} \qquad (1)$$
$$(i_A = i_B = i_C = 1)$$

$$\Delta\varepsilon = \frac{1}{2}\frac{K_{eq}\cdot\Delta\sigma_{ni}}{E}\left(\frac{K_{eq}\cdot\Delta\sigma_{ni}}{\Delta\sigma}+1\right)$$

$$\Delta\varepsilon = \frac{\Delta\sigma}{E}+2\left(\frac{\Delta\sigma}{2K'}\right)^{\frac{1}{n'}} \qquad (2)$$

$$\left(i_A / i_B / i_C = 1,2,...,6/1,2,...,8/1,2,...,5\right)$$

The first equations in systems (1) and (2) are two forms of Sinsinio-Birger's curve. The second equation in (1) is the equation of the cyclic stress-strain curve and the second equation in (2) is the equation of Masing's curve [7].

The values of the nominal stresses σ_{ni} and their ranges $\Delta\sigma_{ni}$, used in (1) and (2), were calculated using the following expressions

$$\sigma_{ni}=223\times\left(\frac{Y_i}{100}\right)^2$$

$$\Delta\sigma_{ni}=223\times\left[\left(\frac{Y_i}{100}\right)^2-\left(\frac{X_i}{100}\right)^2\right] \qquad (3)$$

$$\left(i_A/i_B/i_C=1,2,...,6/1,2,...,8/1,2,...5\right)$$

The values of cyclic properties, used in (1) and (2), with a known equivalent stress concentration factor K_{eq}, were taken from Table 2.

The example of the nonlinear stress-strain response at the critical disk point, provoked by the block A, in the case of 13H11N2V2MF steel in heat treatment state, is shown in Fig.4.

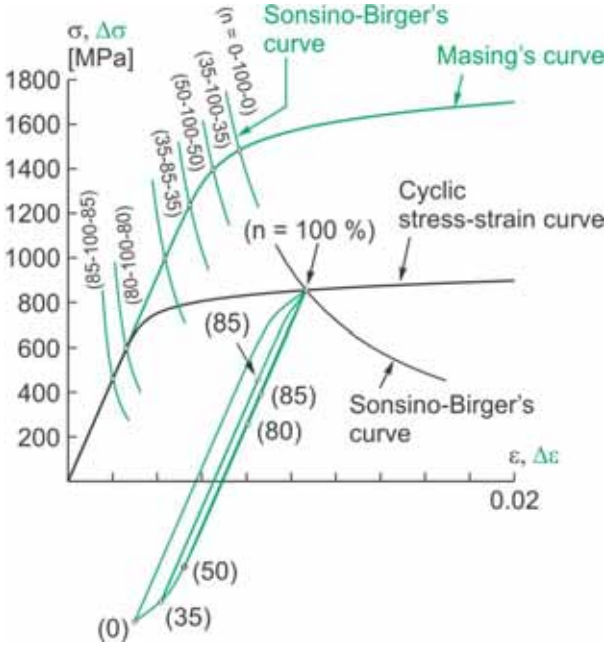

Figure 4. Nonlinear stress-strain response at the critical disk point, provoked by the block A, in the case of 13H11N2V2MF steel in heat treatment state

The first point of the nonlinear stress-strain response at the critical disk point (n=100 %) was obtained using the system of equation (1). The dimensions ($\Delta\varepsilon\times\Delta\sigma$) of stabilized hysteresis loops were obtained using the system of equation (2). The modeling of these hysteresis loops was carried out using corresponding Masing's curves. The numerical results of the nonlinear stress-strain response at the critical disk point are included in Table 3, Table 4 and Table 5. The mean stresses in these tables are marked with σ_{mi}.

Table 3. Numerical results of the nonlinear stress-strain response at the critical disk point provoked by the X-Y-X cycles within the block A

i	$X_i - Y_i - X_i$ [%]	σ_{mi} [MPa]	$\Delta\sigma_i$ [MPa]	$\Delta\varepsilon_i$
13H11N2V2MF steel in delivered state				
1	0-100-0	106.149	1085.673	0.01016932
2	35-100-35	128.664	1040.643	0.00846854
3	50-100-50	158.157	981.656	0.00684357
4	80-100-80	351.909	594.152	0.00290441
5	85-100-85	418.642	460.687	0.00223237
6	35-85-35	50.092	883.498	0.00513218
13H11N2V2MF steel in heat treatment state				
1	0-100-0	112.778	1484.231	0.00768147
2	35-100-35	157.173	1395.440	0.00650403
3	50-100-50	235.722	1238.343	0.00545603
4	80-100-80	555.780	598.227	0.00261026
5	85-100-85	624.315	461.157	0.00201214
6	35-85-35	-42.239	996.615	0.00434976

Table 4. Numerical results of the nonlinear stress-strain response at the critical disk point provoked by the X-Y-X cycles within the block B

i	$X_i - Y_i - X_i$ [%]	σ_{mi} [MPa]	$\Delta\sigma_i$ [MPa]	$\Delta\varepsilon_i$
13H11N2V2MF steel in delivered state				
1	0-100-0	106.149	1085.673	0.01016932
2	70-100-70	249.921	798.129	0.00422408
3	75-100-75	294.500	708.971	0.00356308
4	80-100-80	351.909	594.152	0.00290441
5	85-100-85	418.642	460.687	0.00223237
6	70-95-70	187.661	673.610	0.00334528
7	75-90-75	145.545	411.061	0.00199016
8	70-85-70	43.759	385.805	0.00186740
13H11N2V2MF steel in heat treatment state				
1	0-100-0	112.778	1484.231	0.00768147
2	70-100-70	431.368	847.050	0.00369601
3	75-100-75	491.333	727.121	0.00317266
4	80-100-80	555.780	598.227	0.00261026
5	85-100-85	624.315	461.157	0.00201214
6	70-95-70	350.542	685.396	0.00299058
7	75-90-75	410.124	564.704	0.00246396
8	70-85-70	200.794	385.902	0.00168384

Table 5. Numerical results of the nonlinear stress-strain response at the critical disk point provoked by the X-Y-X cycles within the block C

i	$X_i - Y_i - X_i$ [%]	σ_{mi} [MPa]	$\Delta\sigma_i$ [MPa]	$\Delta\varepsilon_i$
13H11N2V2MF steel in delivered state				
1	0-100-0	106.149	1085.673	0.01016932
2	70-100-70	249.921	798.129	0.00422408
3	75-100-75	294.500	708.971	0.00356308
4	80-100-80	351.909	594.152	0.00290441
5	90-100-90	491.416	291.168	0.00140885
13H11N2V2MF steel in heat treatment state				
1	0-100-0	112.778	1484.231	0.00768147
2	70-100-70	431.368	847.050	0.00369601
3	75-100-75	491.333	727.121	0.00317266
4	80-100-80	555.780	598.227	0.00261026
5	90-100-90	699.721	291.171	0.00127051

Damage at the critical disk point

Damage cases D_A, D_B and D_C provoked by the blocks of rotation frequency A, B and C, of the observed disk, are determined here using Palmgren-Miner's rule of linear damage accumulation [8, 9, 10, 11].

$$D_A = \sum_{i=1}^{6} (D_i)_A = \sum_{i=1}^{6} \left(\frac{N_i}{N_{fi}} \right)_A$$
$$D_B = \sum_{i=1}^{8} (D_i)_B = \sum_{i=1}^{8} \left(\frac{N_i}{N_{fi}} \right)_B \quad (4)$$
$$D_C = \sum_{i=1}^{5} (D_i)_C = \sum_{i=1}^{5} \left(\frac{N_i}{N_{fi}} \right)_C$$

In the above expressions, the damage cases provoked by the X_i–Y_i–X_i cycles, are marked with D_i. These damage cases present the relation between the number of appearance N_i of a particular cycle, and the number N_{fi} of the same cycle where disk material can endure up to the appearance of the initial crack. The number N_i is given in Table 1 and the numbers N_{fi} were determined by solving the systems of equations

$$\frac{\Delta\varepsilon}{2} = \frac{\sigma_f^{'} - \sigma_{mi}}{E} N_f^b + \varepsilon_f^{'} N_f^c$$
$$\frac{\Delta\varepsilon}{2} = \frac{\Delta\varepsilon_i}{2} \quad (5)$$
$$(i_A / i_B / i_C = 1,2,...,6/1,2,...,8/1,2,...,5)$$

The first relation in (5) is Morrow's curve of the LCF in which mean stresses σ_{mi} is included [7, 12-15]. The values $\Delta\varepsilon_i$ in the second equation were taken from Tables 3, 4 and 5. The needed cyclic properties used in system (5) were taken from Table 2. N_i, N_{fi}, D_i, D_A, D_B and D_C data set, for the blocks A, B and C, are included in Tables 6, 7 and 8.

Table 6. Block A: N_i, N_{fi}, D_i and D_A data set

i	$X_i - Y_i - X_i$ [%]	N_i	N_{fi}	D_i
13H11N2V2MF steel in delivered state				
1	0-100-0	1	3308	0.00030230
2	35-100-35	3	5226	0.00057405
3	50-100-50	1	9278	0.00010778
4	80-100-80	2	162040	0.00001234
5	85-100-85	1	495345	0.00000202
6	35-85-35	1	28078	0.00003562
			D_A=	0.00103411
13H11N2V2MF steel in heat treatment state				
1	0-100-0	1	4361	0.00022931
2	35-100-35	3	9141	0.00032819
3	50-100-50	1	20263	0.00004935
4	80-100-80	2	1616158	0.00000124
5	85-100-85	1	8436377	0.00000012
6	35-85-35	1	968810	0.00000103
			D_A=	0.00060924

Table 7. Block B: N_i, N_{fi}, D_i and D_B data set

i	$X_i - Y_i - X_i$ [%]	N_i	N_{fi}	D_i
13H11N2V2MF steel in delivered state				
1	0-100-0	1	3308	0.00030230
2	70-100-70	3	41444	0.00007239
3	75-100-75	2	75107	0.00002663
4	80-100-80	1	162040	0.00000617
5	85-100-85	3	495345	0.00000606
6	70-95-70	1	128512	0.00000778
7	75-90-75	1	2603688	0.00000038
8	70-85-70	1	5644896	0.00000018
			D_B=	0.00042188
13H11N2V2MF steel in heat treatment state				
1	0-100-0	1	4361	0.00022931
2	70-100-70	3	144149	0.00002081
3	75-100-75	2	385402	0.00000519
4	80-100-80	1	1616158	0.00000062
5	85-100-85	3	8436377	0.00000036
6	70-95-70	1	2808943	0.00000036
7	75-90-75	1	1269290413	0.00000000
8	70-85-70	1	8942212789	0.00000000
			D_B=	0.00025664

Table 8. Block C: N_i, N_{fi}, D_i and D_C data set

i	$X_i - Y_i - X_i$ [%]	N_i	N_{fi}	D_i
13H11N2V2MF steel in delivered state				
1	0-100-0	1	3308	0.00030230
2	70-100-70	3	41444	0.00007239
3	75-100-75	1	75107	0.00002663
4	80-100-80	2	162040	0.00000617
5	90-100-90	1	3342689	0.00000090
			D_C=	0.00040838
13H11N2V2MF steel in heat treatment state				
1	0-100-0	1	4361	0.00022931
2	70-100-70	3	144149	0.00002081
3	75-100-75	1	385402	0.00000259
4	80-100-80	2	1616158	0.00000124
5	90-100-90	1	448824959	0.00000000
			D_C=	0.00025395

Systematized data about the damage of the first stage low pressure compressor rotor disk of the R25-300 turbojet engine, in the case of application of 13H11N2V2MF steel in delivered and heat treatment state, for three start-stop cycles (blocks of rotation frequency), are given in Table 9.

Table 9. The data about damage D_A, D_B and D_C in the case of 13H11N2V2MF steel in delivered (DS) and heat treatment state (HTS)

	Damages	Values		
		DS	HTS	
		1	2	1/2
1	D_A	0.00103411	0.00060924	1.70
2	D_B	0.00042188	0.00025664	1.64
3	D_C	0.00040838	0.00025395	1.61
4	$(D_B+D_C)/2$	0.00041513	0.000255295	1.63
1/4		2.49	2.39	

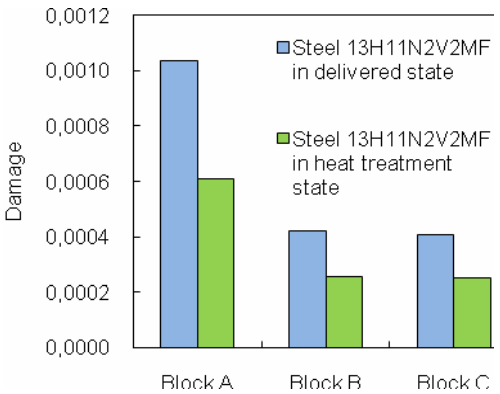

Figure 5. Histogram of the damage

According to Table 9, it can be seen that the damage of our disk, in the case of 13H11N2V2MF steel in delivered state, is significantly higher than the damage in the case of the same steel in heat treatment state. On the other hand, greater differences we have between the damage caused by engine ground controls (block A) and the damage caused by engine flights (blocks B and C). The differences in the damage, presented by a histogram, are given in Fig.5.

Conclusion

The methodology of damage estimation, applied for the first stage low pressure compressor rotor disk of the R25-300 turbojet engine can be applied for all disks dominantly exposed to centrifugal forces of blades and their own centrifugal forces.

This methodology can also be applied for temperature loaded disks. In that case, estimated damage caused by centrifugal forces is one of two or more components of the caused damage.

Monitoring exploitation of turbojet engine disks, for the purpose of turbojet engine maintenance according to the state, should be based on automatic recording of accumulated damage during turbojet engine ground controls and during flights.

In accordance with a rule of linear damage accumulation, turbojet engine disks would be pulled from exploitation with damage equal to one.

The complete results of this paper can serve for further investigations in relation with damage and fatigue life of turbojet engine disks in a function of cyclic material properties and in a function of engine start-stop cycles.

The final goal of designers should be directed to reducing possible damage in critical disk areas using alloys with satisfying cyclic properties.

Ancknowledgments

This work was partial financially supported by the Ministry of Science and Technological Development of Serbia under Projects OI-174001 and TR-35011.

References

[1] POSAVLJAK,S.: *Fatigue Life Investigation of Aero Engine Rotating Disks*, Doctoral dissertation (in Serbian), University of Belgrade, Faculty of Mechanical Engineering, 2008.

[2] KOSTAES,D.: *Fatigue Behavior and Analysis*, Talat Lecture 2401, Technishe Universität München, EAA – European Aluminium Association, 1994.

[3] LAWRI,M.H.: *I-DEAS Master Series*, Mechanical CAE/CAD/CAM Software, Student Guide, Structural Dynamics Research Corporation, SDRC Part Number P-60002, 1998.

[4] SONSINO,C.M.: *Zur Bewertung des Schwingfestig-keitsverhaltens von Bauteilen mit Hilife örtlicher Baunspruchungen*, Konstruktion 45 (1993) 25-33.

[5] SONSINO,C.M.: *Einfluss von Kaltverformungen bis 5% auf das Kurzzeitschwingfestigkeits-verhalten metallischer Werkstoffe*, Dissertation, Vom Fachbereich Machinenbau an der Technischen Hochschule Darmstadt, 1982.

[6] BIRGER,I.A.: (1985) *Prognozirovanie resursa pri malociklovoj ustalosti*, Problemy prochnosti, 1985, No.10, pp.39-44.

[7] BANNATINE,J.A., COMMER,J., HANDROCKJ.: *Fundamentals of Material Fatigue Analysis*, Prentice-Hall, Enlewood Clifs, New Jersey, 1990.

[8] JANKOVIC,M.: *Low Cycle Fatigue* (in Serbian), University of Belgrade, Faculty of Mechanical Engineering, 2001.

[9] PALMGREN,A.: *Die Lebensdauer von Kugellagern, Verfahenstechnik*, Berlin, 68, 1924, pp.339-341.

[10] MINER,M.A.: *Cumulative Damage in Fatigue, Journal of Applied Mechanics*, 1945, 76, A159-164,.

[11] FATEMY,A., YANG,L.: *Cumulative fatigue damage and prediction theories: a survey of the state of the art for homogeneous materials*, International Journal of Fatigue, 1988,Vol.20, No.1, pp.9-34.

[12] MORROW,J.: *Fatigue Design Handbook, Advances in Fatigue*, Vol.4, Society of Automotive Engineers, Warrendale, Pa., Sec 3.2, 1968, pp.21-29.

[13] MAKSIMOVIĆ,S., POSAVLJAK,S., MAKSIMOVIĆ,K., NIKOLIĆ,V., DJURKOVIĆ,V.: *Total Fatigue Life Estimation of Notched Structural Components Using Low-Cycle Fatigue Properties,* J. Strain, Volume 47, Issue Supplement s2, Pages 341-349, December 2011.

[14] POSAVLJAK,S., JANKOVIĆ,M., DJURDJEVIĆ,M.: (2011), *Crack Initiation Life of Turbojet Engine Disks Expressed in Equivalent Cycles*, The 7th International Conference, Research and Development of Mechanical Components and Systems, Proceedings, Pages 253-258, University of Nis, Mechanical Engineering Faculty, April 27th to 28th, Zlatibor, Serbia, 2011.

[15] POSAVLJAK,S., MAKSIMOVIĆ,K., *Initial Fatigue Life Estimation in Aero Engine Discs*, Scientific Technical Review, ISSN 1820-0206, 2011, Vol.61, No.1, pp.25-30.

[16] MAKSIMOVIĆ,K., DJURIĆ,M., JANKOVIĆ,M:, *Fatigue Life Estimation of Damaged Structural Components Under Load* Spectrum, Scientific Technical Review, ISSN 1820-0206, 2011, Vol.61, No.2, pp.16-23.

Received: 24.01.2012

Oštećenje diskova turbomlaznih motora u funkciji od cikličnih karakteristika materijala i vrste motorskog start-stop ciklusa

Oštećenje jednog diska turbomlaznog motora, dominantno izloženog centrifugalnim silama lopatica i sopstvenim centrifugalnim silama, razmatrano je u ovom radu. Pretpostavljeno je da će se za izradu diska koristiti čelik 13H11N2V2MF u isporučenom i termički obrađenom stanju. Jedna lopatica i kritična oblast diska, posmatrani su kao idealno elastična tela. Njihov naponski odziv, za maksimalnu učestanost obrtanja, određen je korišćenjem metoda konačnih elemenata. Ekvivalentni napon u kritičnoj tački diska doveden je u vezu sa ekvivalentnim naponom u odgovarajućoj tački diska kada je isti posmatran kao disk sveden na aksijalno simatričan problem. Na taj način je dobijen takozvani, ekvivalentni faktor koncentracije napona. Ovaj faktor je korišćen za definisanje Sonsino-Birger-ove krive, koja je u kombinaciji sa cikličnim naponsko-deformacionim i Masing-ovim krivima, korišćena za određivanje spektra realnih (elasto-plastičnih) amplituda deformacija u kritičnoj tački diska, za tri različita start-stop ciklusa. Spektar realnih amplituda deformacija, korišćen u tu svrhu, doveden je u vezu sa Morrow-ovim krivima malociklusnog zamora. Oba stanja gore pomenutog čelika poznatih cikličnih karakteristika, uzeta su u obzir.

Ključne reči: **avionski motor, turbomlazni motor, disk, zamor materijala, ciklično opterećenje, koncentracija napona, centrifugalna sila, metoda konačnih elemenata.**

Повреждение дисков турбореактивных двигателей в зависимости от циклических свойств и от видов автомобильных старт-стоп циклов

В этой работе обсуждается повреждение одного диска турбореактивного двигателя, в основном подверженого центробежным силам лезвий лопаток и собственным центробежным силам. Предполагается, что для производства диска будет использоваться сталь 13H11N2V2MF в поставленном и в термически обработанном состоянии. Одна из важнейших и критических областей лопаток и диска рассматриваны идеально упругими телами. Их стрессовая реакция, для максимальной частоты вращения, определяется с использованием метода конечных элементов. Эквивалентные напряжения в критической точке диска были связаны с эквивалентным напряжением в соответствующей точке диска, где диск рассматриван таким же, как диск с осевой симметричной проблемой. Таким образом получен так называемый, эквивалентный коэффициент интенсивности напряжений. Этот фактор используется для определения кривой Сонсино-Биргера, которая была в сочетании с циклическим напряженно-деформированными кривыми и с кривыми Мазинга, и которая была использована для определения спектра реальных (упруго-пластических) амплитуд деформаций в критической точке на диске, для трёх отличающихся старт-стоп циклов. Спектр действительных амплитуд напряжений, используемых для этой цели, был связан с кривыми низкоциклической Морроу усталости. Оба состояния вышеупомянутого стального листа известных циклических характеристик приняты во внимание.

Ключевые слова: **авиационный двигатель, турбореактивный двигатель, привод, усталость материала, циклическая нагрузка, концентрация напряжений, центробежная сила, метод конечных элементов.**

Endommagements des disques chez les turboréacteurs en fonction des propriétés cycliques des matériaux et du type de start stop cycle de moteur

L'endommagement d'un disque du turboréacteur, exposé aux forces centrifuges des lames et aux propres forces centrifuges, a été considéré dans ce travail. On a supposé que pour la fabrication du disque serait utilisé l'acier 13H11N2V2MF à l'état délivré et traité thermiquement. On a observé une lame et le domaine critique de disque comme les corps élastiques idéals. Leur réponse de tension, pour la fréquence maximale de rotation, a été déterminée par la méthode des éléments finis. La tension équivalente au point critique de disque est mise en relation avec la tension équivalente au point correspondant de disque quand il est observé comme le disque réduit au problème axial symétrique. On a obtenu ainsi un soi-disant facteur équivalent de la concentration de tension. Ce facteur a été utilisé pour définir la courbe Sonsino-Birger. Cette courbe, en combinaison avec les courbes cycliques de déformation de la tension de Masing , a été employée pour la détermination du spectre des amplitudes réelles (élastiques plastiques) chez les déformations au point critique de disque, pour trois différents cycles start stop. Le spectre des amplitudes réelles de déformation, employé dans ce but, est mis en relation avec les courbes de fatigue de faible cycle de Morrow. Les deux états de l'acier cité, de caractéristiques cycliques connues, ont été pris on considération.

Mots clés: **moteur d'avion, turboréacteur , disque, fatigue de matériel, charge cyclique, concentration de charge, force centrifuge, méthode des éléments finis.**